Ultrasound in Med. & Biol., Vol. 48, No. 4, pp. 675–684, 2022

0301-5629/$ - see front matter

https://doi.org/10.1016/j.ultrasmedbio.2021.12.009

● *Original Contribution*

A PRELIMINARY STUDY OF LIVER FAT QUANTIFICATION USING REPORTED ULTRASOUND SPEED OF SOUND AND ATTENUATION PARAMETERS

JUVENAL ORMACHEA, and KEVIN J. PARKER
Department of Electrical and Computer Engineering, University of Rochester, Rochester, New York, USA

(*Received* 2 *September* 2021; *revised* 7 *December* 2021; *in final form* 8 *December* 2021)

Abstract—The quantification of liver fat as a diagnostic assessment of steatosis remains an important priority for non-invasive imaging systems. We derive a framework in which the unknown fat volume percentage can be estimated from a pair of ultrasound measurements. The precise estimation of ultrasound speed of sound and attenuation within the liver is found to be sufficient for estimating fat volume assuming a classic model of the properties of a composite elastic material. In this model, steatosis is represented as a random dispersion of spherical fat vacuoles with acoustic properties similar to those of edible oils. Using values of speed of sound and attenuation from the literature in which normal and steatotic livers were studied near 3.5 MHz, we describe agreement of the new estimation method with independent measures of fat. This framework holds the potential for translation to clinical scanners with which the two ultrasound measurements can be made and used for improved quantitative assessment of steatosis. (E-mail: kevin.parker@rochester.edu) **© 2021 World Federation for Ultrasound in Medicine & Biology. All rights reserved.**

Key Words: **Speed of sound, Viscoelasticity, Attenuation, Steatosis, Compressional ultrasound waves.**

INTRODUCTION

Two historic circumstances have motivated a renewed effort to quantify the amount of fat in liver and thereby assess the progression of steatosis with some degree of accuracy. The first motivating factor is the increasing prevalence of fatty liver across the globe, including in younger individuals (Browning et al. 2004; Diehl and Day 2017). The second factor is the increasing capabilities of ultrasound scanners to measure parameters related to compression and shear wave phenomena. These have resulted in a number of techniques and metrics, which are reviewed in recent publications (Pirmoazen et al. 2020; Ferraioli et al. 2021). Generally speaking, a traditional approach is to correlate a single parameter, such as the speed of sound for example, against a steatosis grade in some population as defined by some independent standard. Histology assessments from liver biopsy have been typically used as a gold standard but these are frequently scored with subjective ratings. More recently, magnetic resonance imaging techniques have gained acceptance as a more quantitative and reliable standard (Caussy et al. 2018). However, the single-parameter correlations suffer from imprecision in measurements, biological variability and the inevitable presence of confounding cofactors that are unmeasured yet can influence the parameter being studied. Multiple parameters measured simultaneously can improve the assessment of the severity of steatosis (Baek et al. 2020a, 2020b, 2020c, 2021; Basavarajappa et al. 2020, 2021).

In addition to these approaches, we argue that consideration of the underlying fundamental biophysics can refine the diagnostic value of measured parameters. Specifically, it has recently been reported (Parker et al. 2018; Parker and Ormachea 2021), under a reasonable set of assumptions and using a model of composite material for steatotic livers, that only two measurements are sufficient to determine two key unknown quantities: the background modulus of the liver (which can vary in different disease states) and the volume percentage of fat (distributed in the form of small vacuoles). The sufficient measurements are either the shear wave speed and attenuation or the ultrasound (compressional wave) speed of sound and attenuation. Although this framework has been tested using results from a human clinical trial with shear wave measurements (Parker and Ormachea 2021), there is a need for a more extensive examination of

Address correspondence to: Kevin J. Parker, University of Rochester, Computer Studies Building 724, Box 270231, Rochester, NY 14627-0231, USA. E-mail: kevin.parker@rochester.edu

ultrasound compression wave measures for their predictive value in our model of steatosis. To accomplish that goal, this article reviews first the key equations and assumptions leading to a quantitative model of steatosis and the solutions to two equations with two unknowns. Next, a group of reported measurements of speed of sound (SoS) and attenuation are collected from the literature with a focus on ultrasound around 3.5 MHz, which is common in human abdominal studies. Then, these measurements or their median values are paired and assessed in both the forward model, by way of a nomogram, and the inverse model, by way of regularized optimization of the model equations. The results exhibit reasonable agreement against magnetic resonance imaging (MRI) steatosis estimates and steatosis stages across a number of studies. These preliminary results highlight the potential for routine ultrasound quantification of liver steatosis using scanners capable of accurate speed of sound and attenuation measurements.

THEORY

Composite inclusion model

The accumulation of fat in a liver is generally in the form of small spherical vesicles within the liver hepatocytes. As the vesicles grow in number, our biophysical models predict changes in scattering (Baek et al. 2020b) and biomechanical properties (Parker et al. 2018; Parker and Ormachea 2021). Recently we found (Parker and Ormachea 2021) that the complex (elastic and lossy) hepatic viscoelastic properties could be quantitatively related to the volume percentage of fat. The steatotic liver is modeled as a composite material where the baseline properties are set by normal lean liver. We assume the normal lean liver has a fat content near zero and has well-defined viscoelastic properties (Zhang et al. 2007; Parker et al. 2018). A strong viscous or loss term is linked to fat volume fraction V. The general model of composite medium was originally derived in a landmark paper by Christensen (1969). By imposing the principle of minimum strain energy in a deformed elastic medium, and assuming the inhomogeneities are spherical inclusions, Christensen derived bounds for the effective bulk and shear moduli for the limiting cases of the volume fraction V of spheres being small, or more generally $V <$ 0.5. The effective bulk modulus was derived in eqn (14) of Christensen's (1969) theory. With this model, the composite liver representing simple steatosis will have a bulk modulus B_c given by

$$\frac{B_c}{B_{\text{liver}}} = 1 + \frac{3(1-\nu_1)\left(\frac{B_{\text{fat}}}{B_{\text{liver}}} - 1\right)V}{2(1-2\nu_1) + (1+\nu_1)\left[\frac{B_{\text{fat}}}{B_{\text{liver}}} - \left(\frac{B_{\text{fat}}}{B_{\text{liver}}} - 1\right)V\right]} \tag{1}$$

where B_{liver} represents the bulk modulus of the normal liver, and B_{fat} is the bulk modulus of the fat vacuoles.

Considering that Poisson's ratio of the surrounding matrix approaches the incompressible limit (Fung 1981), $\nu_1 \approx 0.5$, and writing the frequency dependence explicitly, we find that

$$B_c(\omega) \approx \frac{B_{\text{liver}}(\omega) \cdot B_{\text{fat}}(\omega)}{B_{\text{fat}}(\omega) + (B_{\text{liver}}(\omega) - B_{\text{fat}}(\omega))V} \tag{2}$$

where ω is the radial frequency of the ultrasound waves. Equation (2) assumes a small volume fraction of fat V (triglyceride-filled spherical vacuoles) contained within the viscoelastic normal liver, where the normal liver and fat vacuoles are represented by bulk moduli, $B_{\text{liver}}(\omega)$ and $B_{\text{fat}}(\omega)$, respectively.

Composite inclusion model and its relationship with the speed of sound and attenuation parameters

Once $B_c(\omega)$ is specified, the storage modulus and loss modulus can be obtained from the real and imaginary parts of $B_c(\omega)$, respectively. Furthermore, the complex wavenumber $\hat{k}$ is related to the bulk modulus (Blackstock 2000; Carstensen and Parker 2014) as

$$\hat{k} = \frac{\omega}{\sqrt{\frac{B_c(\omega)}{\rho}}} = \frac{\omega}{c_l} - i\alpha \tag{3}$$

where c_l is the ultrasound phase velocity (or commonly the SoS), α is the ultrasound attenuation and ρ is the mass density (assumed to be approximately 1 g/cm^3 for soft tissues). In practice, the speed of sound and attenuation can now be measured using several advanced clinical imaging platforms (Dioguardi Burgio et al. 2019; Ferraioli et al. 2021). Assuming c_l and α have been measured accurately, it is then possible to determine $B_c(\omega)$ as

$$B_c(\omega) = \frac{\rho\omega^2}{\left(\frac{\omega}{c_l} - i\alpha\right)^2} \tag{4}$$

The inverse problem approach

The key clinical question is how V can be determined experimentally. Let us define the complex bulk modulus for normal liver and fat asc

$$B_{\text{liver}}(\omega) = B_{1_{\text{Re}}} + iB_{1_{\text{Im}}} \qquad B_{\text{fat}}(\omega) = B_{2_{\text{Re}}} + iB_{2_{\text{Im}}} \tag{5}$$

Rewriting eqn (2), we have

$$B_c = \frac{(B_{1_{\text{Re}}} + iB_{1_{\text{Im}}})(B_{2_{\text{Re}}} + iB_{2_{\text{Im}}})}{(B_{2_{\text{Re}}} + iB_{2_{\text{Im}}}) + ((B_{1_{\text{Re}}} + iB_{1_{\text{Im}}}) - (B_{2_{\text{Re}}} + iB_{2_{\text{Im}}}))V} \tag{6}$$

This can be separated into two equations, one real part and another imaginary part. By separating these terms, the real part of the composite $\mathrm{Re}[B_c]$ and the imaginary part $\mathrm{Im}[B_c]$ can be identified:

$$\begin{aligned}\mathrm{Re}[B_c] &= \frac{B_{1_{Re}}\left(B_{2_{Re}}^2+B_{2_{Im}}^2\right)(1-V)+\left(B_{1_{Re}}^2B_{2_{Re}}+B_{1_{Im}}^2B_{2_{Re}}\right)V}{B_{2_{Re}}^2+B_{2_{Im}}^2-2\left(B_{2_{Re}}^2-B_{1_{Re}}B_{2_{Re}}+B_{2_{Im}}(B_{2_{Im}}-B_{1_{Im}})\right)V+\left((B_{1_{Re}}-B_{2_{Re}})^2+(B_{1_{Im}}-B_{2_{Im}})^2\right)V^2}\\ \mathrm{Im}[B_c] &= \frac{B_{1_{Im}}\left(B_{2_{Re}}^2+B_{2_{Im}}^2\right)(1-V)+\left(B_{1_{Re}}^2B_{2_{Im}}+B_{1_{Im}}^2B_{2_{Im}}\right)V}{B_{2_{Re}}^2+B_{2_{Im}}^2-2\left(B_{2_{Re}}^2-B_{1_{Re}}B_{2_{Re}}+B_{2_{Im}}(B_{2_{Im}}-B_{1_{Im}})\right)V+\left((B_{1_{Re}}-B_{2_{Re}})^2+(B_{1_{Im}}-B_{2_{Im}})^2\right)V^2}\end{aligned} \tag{7}$$

Let us assume that the parameters for the lossy part of the normal liver and the fat vesicles are known, $B_{1_{Im}}$ and B_{fat}, respectively. In addition, B_c is assumed to be accurately estimated from experimental measurements at a specific frequency ω as in eqn (4). In this particular case we then have two equations in two unknowns, $B_{1_{Re}}$ (real part of B_{liver}) and V (fat volume percentage), that can be solved using numerical methods. In practice, regularization methods are employed to minimize problems of random errors in measurements or parameters that might invalidate the system of equations.

Taking the real and imaginary parts of eqn (4) numerically provides two values for the left-hand side of eqn (7), which can then be solved numerically for $B_{1_{Re}}$ and V. Numerical solution routines search through a parameter space to find the solution, in the form of a global minimum of a corresponding minimization formulation. Thus, the steps for quantifying liver fat volume fraction from ultrasound speed of sound and attenuation measurements are as follows:

- Measure c_l and α. Calculate $B_c(\omega)$ using eqn (4) at a fixed ω.
- Find the real and imaginary parts of the right-hand side of eqn (4).
- Substitute those into eqn (7) for $\mathrm{Re}[B_c]$ and $\mathrm{Im}[B_c]$ with *a priori* known $B_{1_{Im}}$ and B_{fat}.
- Solve numerically for $B_{1_{Re}}$ and V. Also, calculate B_{liver} using eqn (5).

METHODS

To assess the validity of the theoretical model, we examined literature reports for SoS and attenuation and then applied these to the inverse solution algorithm and the nomogram.

Speed of sound in vivo *liver: Literature review*

Conventionally, medical ultrasound systems assume an SoS for transmit and receive beamforming operations. The assumed SoS is typically held constant, usually at 1540 m/s for the entire image. However, because of this assumption, the ultrasound image quality may have a degradation because the different organs may have different SoSs (Jaeger et al. 2015). Multiple studies have measured hepatic SoS *in vivo* as a non-invasive biomarker for liver steatosis. In this work, we reviewed different articles that reported SoS measurements for liver tissue based on four techniques: focusing, spatial coherence, compounding and single-path transmission. The first three selected methods were recently considered the most promising categories for SoS measurements (Wang et al. 2021). The number of reviewed articles for each of these methods was 3. Table 1 gives more details on the reviewed references for SoS measurements.

Attenuation in vivo *liver: Literature review*

The attenuation coefficient (AC) measures the acoustic energy loss when an ultrasound signal passes through a medium. Different approaches to measuring the AC have been proposed by many researchers over several decades (Ferraioli et al. 2021). These techniques analyze the radiofrequency (RF) echo signals detected by the transducer. Some of the proposed methods are the

Table 1. Literature review for hepatic speed of sound and steatosis

Authors	Speed of sound (m/s)				Frequency (MHz)	Method
	S0	S1	S2	S3		
Boozari et al. (2010)	1575 ± 21	NRV	NRV	NRV	2–5	Focusing
Napolitano et al. (2006)	1480	NRV	NRV	NRV	4	Focusing
Hayashi et al. (1988)	1538 ± 29	NRV	NRV	NRV	3.5	Focusing
Imbault et al. (2017)	1557	1553	1551	NRV	1–6	Spatial coherence
Imbault et al. (2018)	1570	1510	NRV	1470	1–6	Spatial coherence
Dioguardi Burgio et al. (2019)	1570 ± 26	1533 ± 26	1511	1481 ± 13	3.5	Spatial coherence
Stähli et al. (2020)	1564 ± 4	NRV	NRV	NRV	5	Compounding
Robinson et al. (1982)	1574 ± 15	NRV	NRV	NRV	3	Compounding
Chen et al. (1987)	1578 ± 5.4	NRV	NRV	NRV	3.5	Compounding
Shigemoto et al. (2001)	1585	NRV	NRV	NRV	2.5	Single-path transmission measurement
Lin et al. (1987)	1574 ± 10.4	1565 ± 8.3	1548	1538	5	Single-path transmission measurement
Bamber and Hill (1981)	1573	NRV	NRV	NRV	1–7	Single-path transmission measurement

NRV = no reported value.

spectral shift, spectral difference, spectral log difference and hybrid methods (Bigelow and Labyed 2013). Thus, the AC has been used as a surrogate parameter for hepatic fat quantification. In this work, we report AC results for *in vivo* liver patients using commercial implementations of SoS and AC estimation in different ultrasound clinical systems. The numbers of reviewed articles were: 4 using the 2-D attenuation imaging (ATI) system (Aplio i800, Canon Medical Systems, Otawara, Japan), 3 applying the attenuation parameter (ATT) system (Aloka-Arietta, Fujifilm, previously Hitachi Ltd., Japan), 2 using the ultrasound-guided attenuation parameter (UGAP) system (LOGIQ E9, General Electric, Schenectady, NY, USA), 1 using the diagnostic system (EPIQ-7G, Philips, Bothell, WA, USA) and 1 using the tissue attenuation imaging (TAI) system (RS85, Samsung Medison, Seoul, Korea). We were not able to extract the AC parameter from the ultrasound-derived fat fraction (UDFF) system (Acuson S3000, Siemens Healthineers, Erlangen, Germany) as this product directly reports its estimated fat fraction percentage. Table 2 gives more details on the reviewed references for AC measurements. For the study using the Samsung system, Jeon et al. (2021) reported TAI values based on visual steatosis grades and the controlled attenuation parameter. Thus, we included the mean and standard deviation of TAI values, in Table 2, based on both grades.

Solution by nomogram

A nomogram can be employed as a simplified graphical solution approach. To generate a nomogram, the forward solution is calculated from eqns (2)–(4), and the resulting theoretical values of c_l and α are plotted on a graph, with contours representing regular increments of $\{V, B_{1_{\mathrm{Re}}}\}$ values. Then, any measured pair of $\{c_l, \alpha\}$ can specify a unique point location within the contours, which provides an immediate graphical estimate of the corresponding $\{V, B_{1_{\mathrm{Re}}}\}$. As an example, see Figure 1. Any patient data that fall outside of the contour ranges would indicate that there were possible errors in the measurements or that some model parameters need to be adjusted. The reader should also note that units for AC are Nepers per centimeter (Np/cm) at 3.5 MHz. In general, the AC units used to estimate the bulk modulus must be specified at a selected ultrasound frequency or center frequency used for analysis. The conversion from AC units reported in the literature to Np/cm is possible using 1 Np $\approx$ 8.68 dB.

Solution by the inverse problem

Our numerical solution for V and $B_{1_{\mathrm{Re}}}$ using a minimization approach subtracts the magnitude of the terms of the next equation. This should approach zero as the correct values of V and $B_{1_{\mathrm{Re}}}$ are determined within the system of equations. The real and imaginary parts are equally weighted, although this may be varied in future research. We also limit the search parameter within practical ranges, and simulated annealing is employed to avoid the issue of entrapment within local minima. In summary, our specific routine to find the minimum solution T is

$$\begin{aligned} \underline{\mathrm{Min}} T = {} & \left|\mathrm{Re}\left[B'_{\mathrm{m}}\right] - \mathrm{Re}[B_{\mathrm{c}}]\right| + \left|\mathrm{Im}\left[B'_{\mathrm{m}}\right] - \mathrm{Im}[B_{\mathrm{c}}]\right| \\ & \underline{\text{subject to}} \\ 0.001 < {} & V < 0.65 \\ 1.9\,\mathrm{GPa} < {} & B_{1_{\mathrm{Re}}} < 2.6\,\mathrm{GPa} \\ 0.95\mathrm{Re}[B_{\mathrm{m}}] < {} & \mathrm{Re}\left[B'_{\mathrm{m}}\right] < 1.05\mathrm{Re}[B_{\mathrm{m}}] \\ 0.95\mathrm{Im}[B_{\mathrm{m}}] < {} & \mathrm{Im}\left[B'_{\mathrm{m}}\right] < 1.05\mathrm{Im}[B_{\mathrm{m}}] \end{aligned} \tag{8}$$

where B_{m} is obtained from the measured c_l and α using eqn (4) and where B'_{m} is the approximate composite modulus entered into the equation. In the numerical search algorithm, the real and imaginary parts of B'_{m} are

Table 2. Literature review for hepatic attenuation coefficient and steatosis

Authors	Attenuation coefficient (dB/cm/MHz)				Frequency (MHz)	System
	S0	S1	S2	S3		
Jeon et al. (2019)	0.58	0.65	0.73	0.73	1–8	ATI-Canon
Yoo et al. (2020)	0.55 ± 0.08	0.66 ± 0.08	0.76 ± 0.09	0.76 ± 0.09	1–8	ATI-Canon
Dioguardi Burgio et al. (2020)	0.63 ± 0.09	0.71 ± 0.11	0.87 ± 0.09	0.87 ± 0.09	3	ATI-Canon
Ferraioli et al. (2019)	0.56	0.68	0.85	0.85	1–8	ATI-Canon
Cerit et al. (2020)	0.56	0.62	0.73	0.73	1–6	ATT- Fujifilm/Hitachi
Koizumi et al. (2019)	0.57	0.63	0.72	0.72	1–5	ATT- Fujifilm/Hitachi
Tamaki et al. (2018)	0.55	0.63	0.69	0.69	1–5	ATT- Fujifilm/Hitachi
Fujiwara et al. (2018)	0.49	0.56	0.66	0.66	4	UGAP-GE
Tada et al. (2020)	0.53	0.65	0.78	0.78	4	UGAP-GE
D'Hondt et al. (2021)	0.48 ± 0.08	0.54 ± 0.03	0.57 ± 0.04	0.57 ± 0.04	1–5	Philips
Jeon et al. (2021)	0.66 ± 0.05	0.75 ± 0.07	1.11 ± 0.13	0.88 ± 0.09	1–7	TAI-Samsung
Jeon et al. (2021)	0.69 ± 0.07	0.81 ± 0.07	0.85 ± 0.12	1.03 ± 0.13	1–7	TAI-Samsung

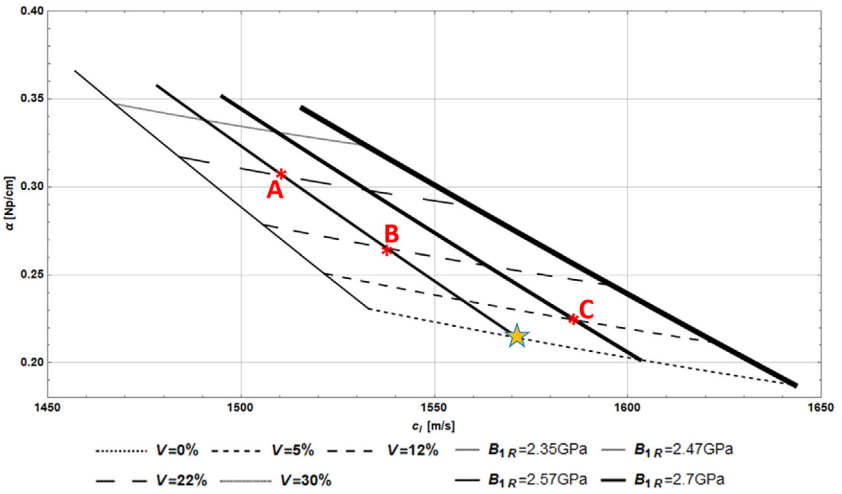

Fig. 1. Nomogram providing graphical estimates of fat volume fraction V and liver matrix bulk modulus $B_{1_{\mathrm{Re}}}$, given measurements of the attenuation coefficient (AC, vertical axis) and speed of sound (SoS, horizontal axis) and assuming a frequency of 3.5 MHz. The 2-D parametric space is illustrated with particular values of V from 0% to 30% (*dashed lines*) and also for particular increasing values of $B_{1_{\mathrm{Re}}}$ (*solid lines*). Any measured liver values of attenuation and speed can be plotted on the nomogram to provide a graphical estimate of the V and $B_{1_{\mathrm{Re}}}$, values for that liver. For example, given three pairs of $\{c_l, \alpha\}$ points A, B and C, their corresponding $\{V, B_{1_{\mathrm{Re}}}\}$ would be {22%, 2.47 GPa}, {12%, 2.47 GPa} and {5%, 2.57 GPa}, respectively. The *yellow star point* illustrates the assumed $\{c_l, \alpha\}$ for a normal liver with very low fat and measured at 3.5 MHz.

allowed to have a few percent variations from the measured modulus B_{m} (because of the imprecision of measurements), as indicated in the lower two lines of eqn (8). In these expressions, the two unknowns are $B_{1_{\mathrm{Re}}}$ (the real part of the liver's bulk modulus) and V (the volume fraction of fat vesicles), which are linked to the composite modulus. The simulated annealing algorithm searches within constraints on the permitted values of V and $B_{1_{\mathrm{Re}}}$: $0.001 < V < 0.65$ and 1.9 GPa $< B_{1_{\mathrm{Re}}} <$ 2.6 GPa. The upper limit, V_{h}, for V was defined with one additional practical criterion: if the ratio $\mathrm{Im}[B'_{\mathrm{m}}]/\mathrm{Re}[B'_{\mathrm{m}}]$ was lower than 0.004 (essentially approaching a purely elastic material), then $V_{\mathrm{h}} = 0.4$, else $V_{\mathrm{h}} = 0.65$ otherwise. In other words, the search constraint on V is restricted when the imaginary part is very low. The particular value of $V_{\mathrm{h}} = 0.65$ is not critical, simply representing a practical upper limit to the values of fat percent that have been reported. To match the literature review data for SoS and AC, we assumed a frequency of 3.5 MHz, an imaginary part of 7.56 MPa for normal liver and a complex bulk modulus B_{fat}= 1.8 GPa + i12.9 MPa. The reasoning to select these values, for $B_{1_{\mathrm{Im}}}$and B_{fat}, respectively, is presented in the next section. After $B_{1_{\mathrm{Re}}}$ is obtained, B_{liver} is calculated using eqn (5) with $B_{1_{\mathrm{Im}}} = 7.56$ MPa. Using the "NMinimize" function in Mathematica (Version 12.1.1.0, Wolfram, Champaign, IL, USA), the numerical solution representing the global minimum is obtained from the following command:

$$\begin{aligned}&\mathrm{NMinimize}\\&\quad[\{\mathrm{T}, \mathrm{constraints}\}, \{\mathrm{V}, \mathrm{B}_{1_{\mathrm{Re}}}, \mathrm{Re}[\mathrm{B'_m}], \mathrm{Im}[\mathrm{B'_m}]\},\\&\qquad \mathrm{Method} \rightarrow {}^{''}\mathrm{SimulatedAnnealing}^{''}]\end{aligned} \tag{9}$$

Randomization of SoS and AC pairs based on literature results

To assess the variability within the nomogram approach and the inverse problem solution, we generated nine random pairs of SoS and AC selected from the middle quartiles of each steatosis group: normal (S0), S1, S2 and S3. For example, normal liver SoS and AC values are in the ranges 1540−1570 m/s and 0.4−0.7 dB/cm/MHz, respectively. Thus, we randomly selected nine SoS and AC values for each range and generated nine pairs, for example {1565 m/s, 0.56 dB/cm/MHz}, representing each steatosis score. Moreover, the median SoS values reported by Dioguardio Burgio et al. (2019) and the median AC values reported by Ferraioli et al. (2019) were selected to form four additional pairs (one for each steatosis score). We selected these particular values because both studies compared their results against a fat fraction value that is given by the magnetic resonance imaging proton density fat fraction (MRI-PDFF) parameter. MRI-PDFF is considered an alternative, non-invasive, gold standard method for liver fat quantification and hepatic steatosis staging. Thus, we simulated 40

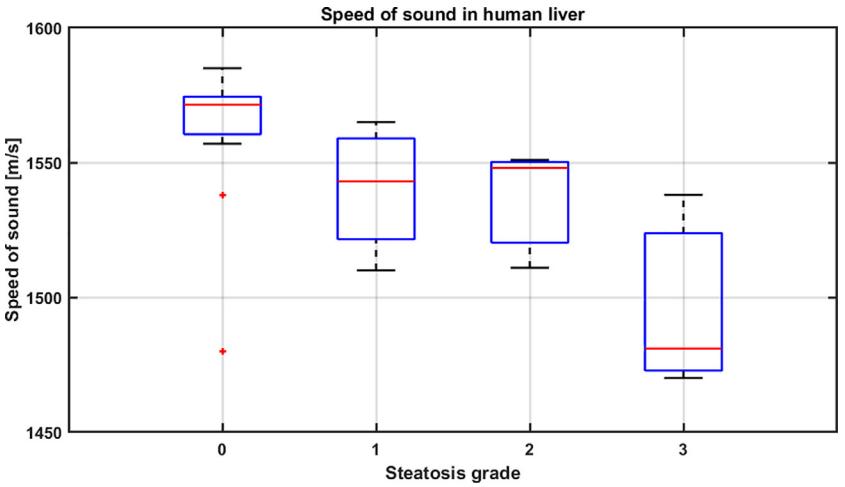

Fig. 2. Boxplot indicating the median speed of sound values and interquartile range for each steatosis stage obtained from the literature review from different studies reporting hepatic speed of sound versus steatosis stage. Each *box* represents values from the lower to upper quartile (25th −75th percentiles). The *middle line* represents the median values. A *vertical line* extends from the minimum to the maximum range. Separate *red points* represent the excluded outlier values. The review data are outlined in Table 1.

measurements of SoS and AC for *in vivo* liver patients that are properly bounded by clinical studies reported in the literature, as entry values for the nomogram and the numerical inverse solution.

RESULTS

Speed of sound

Overall, hepatic SoS varied from 1470 to 1590 m/s depending on the underlying pathology. Normal liver SoS was approximately 1570 m/s, while fatty livers had lower SoS values. While Bamber and Hill (1981), Chen et al. (1987) and Hayashi et al. (1988) did not report SoS values for S1, S2 and S3 scores, they reported SoS values of 1547 ± 17.8, 1423 ± 34 and 1556 m/s for fatty liver tissue, respectively. Figure 2 illustrates and summarizes the hepatic SoS values reported in the literature for normal, S0, S1, S2 and S3 steatosis stages.

Attenuation coefficient

On the basis of the literature review, the AC of liver ranges from 0.48 to 1.11 dB/cm/MHz. The AC values for normal liver fall within the range of 0.48 to 0.69 dB/cm/MHz, whereas the AC value falls in the ranges of 0.54 to 0.81 dB/cm/MHz, 0.57 to 0.88 dB/cm/MHz and 0.72 to 1.11 dB/cm/MHz for the S1, S2 and S3 stages, respectively. Figure 3 illustrates and summarizes the hepatic AC values reported in the literature for normal, S0, S1, S2 and S3 steatosis stages.

Composite modulus for normal liver and fat

A bulk modulus for normal liver was assumed based on the median values of SoS (1570 m/s) and AC (0.55 dB/cm/MHz) obtained from the S0 (normal) group in Figures 1 and 2. Then, a normal $B_{\text{liver}} = 2.46$ GPa $+ i$ 7.56 MPa was obtained using eqn (4). Thus, $B_{1_{\text{lm}}}$ is equal to 7.56 MPa. For the fat bulk modulus case, we used an SoS of 1400 m/s based on the work by Azman and Abd Hamid (2017) determining the SoS of different types of edible oils, and we used an AC of 1.39 dB/cm/MHz based on the studies by Chanamai and McClements (1998) and Ghosal et al. (2012) evaluating edible oils and fatty livers, respectively, and we used a density value of 0.92 g/cm^3 (Abe et al. 2020). If these values are assumed and eqn (4) is used, B_{fat}= 1.8 GPa + i12.9 MPa. Therefore, we retained these values, $B_{1_{\text{lm}}}$ and B_{fat}, as constants for the inverse problem solution.

Results from randomized SoS and AC pairs

The 40 randomized values of SoS and AC pairs were clustered around the measurements reported in clinical studies and were used as ersatz measurements from liver patients. These were entered as inputs into the nomogram and the numerical inverse solution. Both approaches produced bounded estimates of fat percentages as shown in the following sections.

Nomogram

Figure 4 illustrates individual pairs of SoS and AC values on the nomogram. Curves indicate the fat volume fraction V at increasing values, which generally correspond to increasing grades of steatosis. V values correspond to similar fat cutoff values in studies that measure MRI-PDFF: S0 ≤6.5%, S1 <16.5%, S2 <22% and S3 ≥22% (Dioguardi Burgio et al. 2019; Ferraioli et al. 2019).

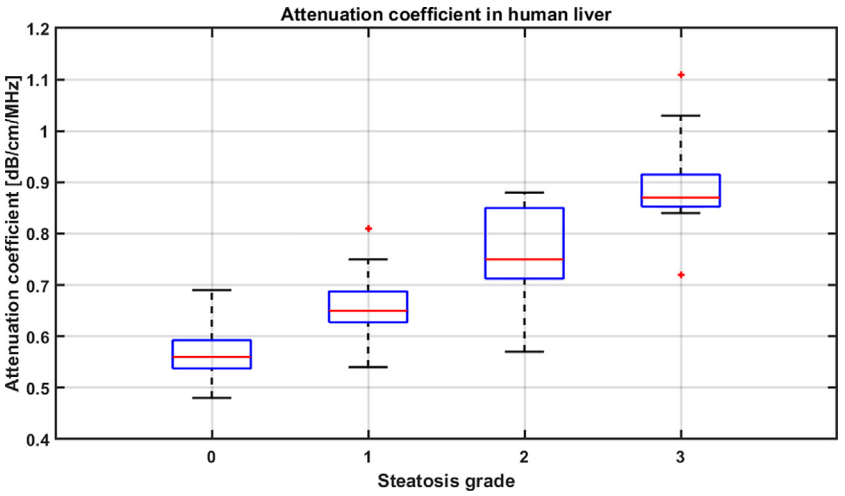

Fig. 3. Boxplot indicating the median attenuation coefficient values and interquartile range for each steatosis stage obtained from the literature review from different studies reporting hepatic attenuation coefficient versus steatosis stage. Each *box* represents values from the lower to upper quartile (25^{th}–75^{th} percentile). The *middle line* represents the median values. A *vertical line* extends from the minimum to the maximum range. Separate *red points* represent the excluded outlier values. The review data are outlined in Table 2.

Inverse solution

Figure 5 illustrates the numerical estimates from the 40 selected pairs of SoS and AC within the literature review indicating the estimated volume percentage V of fat as a function steatosis stages S0 to S3. A steady increase in estimated V is observed. The median values for each group are 6% (S0), 13.5% (S1), 19.3% (S2) and 21.3% (S3). The *diamond points* for each boxplot are the calculated V using the median SoS and AC values from Dioguardio Burgio et al. (2019) and Ferraioli et al. (2019), respectively. For these four $\{c_l, \alpha\}$ pair points, V is equal to 7% (S0), 13% (S1), 19% (S2) and 23% (S3);

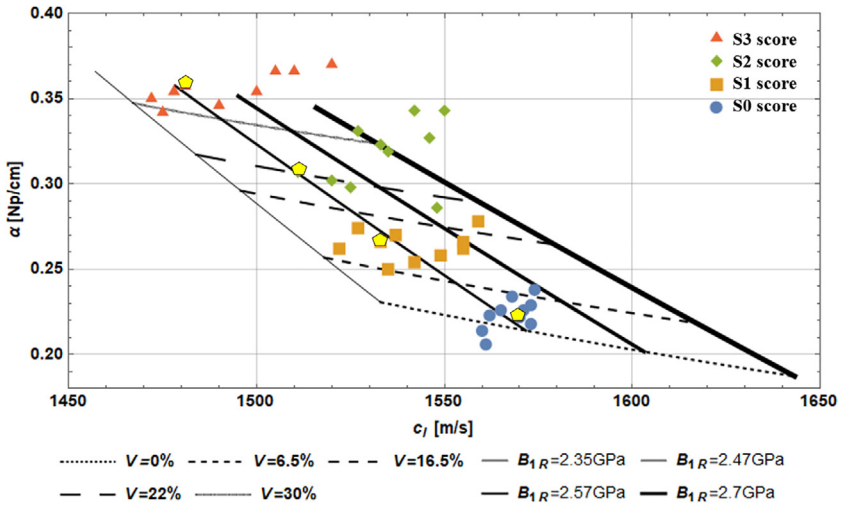

Fig. 4. Sensitivity of theory versus experiments, revealing the randomly selected $\{c_l, \alpha\}$ pair points from within steatosis scores of S0 (*blue circles*), S1 (*orange squares*), S2 (*green diamonds*) and S3 (*red triangles*). Theoretical *dashed-line curves* represent values of V equal to 0%, 6.5%, 16.5%, 22% and 30% covering different liver bulk modulus values, $B_{1_{Re}}$, between 2.35 and 2.7 GPa. The selected data are found to be stratified such that the 10 cases of S3 are located above or near the $V = 30\%$ curve. Most of the S2 cases are located between $V = 16.5\%$ and 30% curves. Most of the S1 cases are below the $V = 16.5\%$ curve, and most of the S0 points are below $V = 6.5\%$. These V ranges are in agreement with the magnetic resonance imaging proton density fat fraction steatosis grade used in Dioguardi Burgio et al. (2019): S0 $\leq$6.5%, S1 $<$16.5%, S2 $<$22% and S3 $\geq$22%. The *yellow pentagons* represent the median speed of sound and attenuation coefficient values from Dioguardi Burgio et al. (2019) and Ferraioli et al. (2019), respectively. For these four $\{c_l, \alpha\}$ pair points, V is close to 3%, 12% and 22%, and higher than 30% with normal bulk liver $B_{1_{Re}} = 2.47$ GPa.

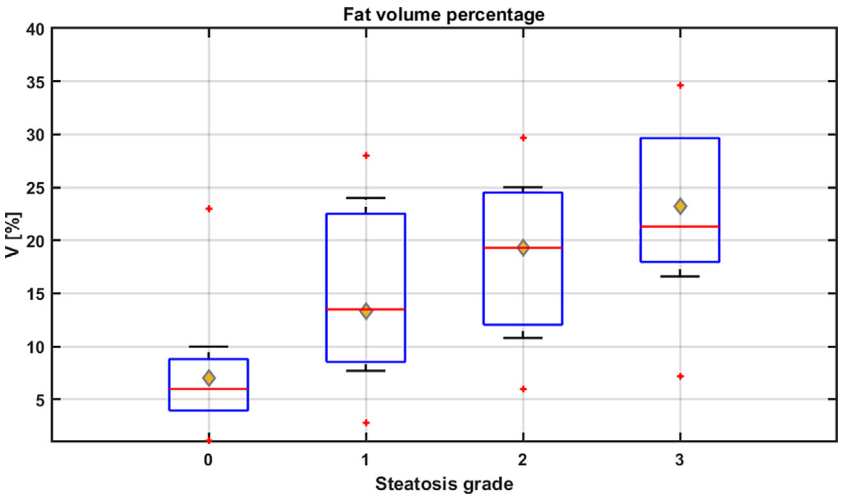

Fig. 5. Numerical solution of volume percentage fat V from the 40 randomly selected pairs of attenuation coefficient and speed of sound. The steady increase in estimated V is observed. The *diamond points*, at each boxplot, are the calculated V using the median speed of sound and attenuation coefficient values from Dioguardi Burgio et al. (2019) and Ferraioli et al. (2019), respectively. For these four $\{c_l, \alpha\}$ pair points, V equals 7%, 13%, 19% and 23%; these V values agree with the magnetic resonance imaging proton density fat fraction steatosis grade used in these two studies: S0 $\leq$6.5%, S1 $<$16.5%, S2 $<$22% and S3 $\geq$22%. Separate *red points* represent the excluded outlier values for each score.

these V values agree and correlate with the similar MRI-PDFF steatosis grades used in these two studies: S0 $\leq$6.5%, S1 $<$ 16.5%, S2 $<$ 22% and S3 $\geq$22%.

DISCUSSION

Both the nomogram approach and the inverse numerical solution approach produce reasonable agreement with independent assessments of hepatic fat. In particular, MRI-PDFF assesses the concentration of mobile triglycerides within the hepatic tissue (Caussy et al. 2018). It is an imaging biomarker that has excellent diagnostic value for assessment of hepatic fat content in patients with non-alcoholic fatty liver disease (NAFLD) (Jayakumar et al. 2019). Several clinical studies have used the parameter and compared it against histological assessments from liver biopsy, finding that MRI-PDFF is highly reproducible, accurate, precise and a reliable biomarker of steatosis (Caussy et al. 2018; Ferraioli et al. 2019; Gu et al. 2019; Jayakumar et al. 2019; Stine et al. 2021; Tada et al. 2020). In addition, unlike liver biopsy, it can be used for longitudinal studies to evaluate liver fat content changes (Jayakumar et al. 2019). Moreover, MRI-PDFF has been used as an alternative reference standard measurement in clinical trials that measure AC (Tada et al. 2020; D'Hondt et al. 2021). Overall, MRI-PDFF reveals a direct correlation between liver fat content and liver steatosis stage. However, clear fat percentage cutoffs and ranges for each steatotic score are not yet defined. Jayakumar et al. (2019) reported median (interquartile) MRI-PDFF ranges of 5.8% (5.2, 6.7), 14.5% (10.3, 19.2), 26.2% (18.2, 29.0) and 32.2% (26.0, 38.4) in patients with S0, S1, S2 and S3 steatosis, respectively. Jeon et al. (2019) reported steatotic MRI-PDFF cutoff values of normal $<$5%, mild 5%$-$10% and moderate and severe $>$10%. Ferraioli et al. (2021) reported MRI-PDFF cutoff values of S0 $<$ 5%, S1 $\leq$16.3%, S2 $<$ 21.6% and S3 $\geq$21.6%. Similarly, Dioguardi Burgio et al. (2019) reported cutoff values of S0 $\leq$6.5%, S1 $\leq$16.5%, S2 $<$ 22% and S3 $\geq$22%. Further studies are needed to better define these ranges; nevertheless, it can be noted that our preliminary fat content V results correlate with these fat percentage ranges. Our estimated median values are 6%, 13.5%, 19.3% and 21.3% for groups S0, S1, S2 and S3, respectively. Furthermore, the estimated fat content, using the median values of SoS and AC from Dioguardi Burgio et al. (2019) and Ferraioli et al. (2021), are in good agreement with the MRI-PDFF threshold values used in both studies. Thus, our approach could be an alternative method to non-invasively assess the *in vivo* hepatic fat content using ultrasound systems that are less expensive, more portable and more widely available globally than MRI systems.

Limitations of this study and the approach include the need for higher precision in the measurements of speed of sound and attenuation and the precise determination of model parameters. As many efforts are ongoing to improve ultrasound measurements and their implementation on clinical scanners, it is anticipated that these will become more accurate and precise over time. However, more physical and mechanical measurements may be required to independently confirm the baseline values

of bulk moduli used in the model. The variability of the bulk moduli of the fat/oil component between individuals is an area requiring further research. Furthermore, the model predicts that fibrosis within a steatotic liver is an important cofactor by means of changing the bulk modulus of the liver; however, this requires further study with independent confirmation of the degree of influence. The studies included in Tables 1 and 2 did not quantify fibrosis and so this remains a parameter requiring additional research for comparison against the predictions of the model. Also, the effects of other cofactors such as inflammation and high blood pressure have not been incorporated. Furthermore, we have centered our study around the common abdominal scanning frequency of 3.5 MHz; however, lower and higher center frequencies are available for obese and thin or small patients, respectively. The results will be strongly dependent on frequency as attenuation in liver is commonly expressed in terms of decibels per centimeter per megahertz (dB/cm/MHz); thus, a factor of 2 change in frequency will result in an (approximately) factor of 2 change in attenuation. In our model this is directly reflected in eqns (3) and (4) and the *a priori* estimate of the bulk modulus of fat in eqn (5). These will require further verification.

It is interesting to compare these results using ultrasound waves and bulk moduli against those obtained recently using shear waves and shear moduli (Ormachea and Parker 2021). The composite model and nomograms for each case have some similarities, but the precision required to accurately determine fat volume percentage V from the measured parameters differs. This is a larger subject that will require further refinement, but it is possible to speculate that a clinical scanner capable of four measurements (speed and attenuation from both ultrasound and shear waves) would be able to improve the final estimation of fat content by using both sets of solutions. This remains for future work as measurement capabilities increase in clinical scanners.

CONCLUSIONS

An analysis of the composite model of hepatic steatosis was performed, and a fat quantification of liver was achieved using the longitudinal (compressional) speed of sound and attenuation coefficient, with results in good agreement with values reported for MRI-PDFF. The composite model approach has the potential to be implemented in commercial clinical systems for rapid steatosis staging. Thus, fat quantification could be achieved in a safe, low-cost ultrasound system. The calculated estimate of liver fat volume percentage V has the potential to be used as a quantitative biomarker for assessing and monitoring liver fat concentration for hepatic steatosis.

Acknowledgments—This work was supported by the Hajim School of Engineering and Applied Sciences and the Department of Electrical and Computer Engineering at the University of Rochester.

Conflicts of Interest—The authors and the University of Rochester have patent applications pending that may pertain to some of the subject matter discussed herein.

REFERENCES

Abe T, Bell ZW, Dankel SJ, Wong V, Spitz RW, Loenneke JP. The water-fat separation method for determining the fat-free component of subcutaneous adipose tissue in humans: A brief review. J Clin Densitom 2020;23:390–394.

Azman NA, Abd Hamid SB. Determining the time of flight and speed of sound on different types of edible oil. IOP Conf Ser Mater Sci Eng 2017;260 012034.

Baek J, Ahmed R, Ye J, Gerber SA, Parker KJ, Doyley MM. H-Scan, shear wave and bioluminescent assessment of the progression of pancreatic cancer metastases in the liver. Ultrasound Med Biol 2020a;46:3369–3378.

Baek J, Poul SS, Swanson TA, Tuthill T, Parker KJ. Scattering signatures of normal versus abnormal livers with support vector machine classification. Ultrasound Med Biol 2020b;46:3379–3392.

Baek J, Swanson TA, Tuthill T, Parker KJ. Support vector machine (SVM) based liver classification: Fibrosis, steatosis, and inflammation. In: Proc 2020 IEEE Int Ultrason Symp. 1–4.

Baek J, Poul SS, Basavarajappa L, Reddy S, Tai H, Hoyt K, Parker KJ. Clusters of ultrasound scattering parameters for the classification of steatotic and normal Livers. Ultrasound Med Biol 2021;47:3014–3027.

Bamber JC, Hill CR. Acoustic properties of normal and cancerous human liver: I. Dependence on pathological condition. Ultrasound Med Biol 1981;7:121–133.

Basavarajappa L, Reddy S, Tai H, Song J, Rijal G, Parker KJ, Hoyt K. Early assessment of nonalcoholic fatty liver disease using multiparametric ultrasound imaging. Proc 2020 IEEE Int Ultrason Symp 2020;1–4.

Basavarajappa L, Baek J, Reddy S, Song J, Tai H, Rijal G, Parker KJ, Hoyt K. Multiparametric ultrasound imaging for the assessment of normal versus steatotic livers. Nat Sci Rep 2021;11:2655.

Bigelow TA, Labyed Y. Attenuation compensation and estimation. In: Mamou J, Oelze ML, (eds). Quantitative ultrasound in soft tissues. : Dordrecht: Springer Netherlands; 2013. p. 71–93.

Blackstock DT. Fundamentals of physical acoustics. New York: Wiley; 2000.

Boozari B, Potthoff A, Mederacke I, Hahn A, Reising A, Rifai K, Wedemeyer H, Bahr M, Kubicka S, Manns M, Gebel M. Evaluation of sound speed for detection of liver fibrosis: Prospective comparison with transient dynamic elastography and histology. J Ultrasound Med 2010;29:1581–1588.

Browning JD, Szczepaniak LS, Dobbins R, Nuremberg P, Horton JD, Cohen JC, Grundy SM, Hobbs HH. Prevalence of hepatic steatosis in an urban population in the United States: Impact of ethnicity. Hepatology 2004;40:1387–1395.

Carstensen EL, Parker KJ. Physical models of tissue in shear fields. Ultrasound Med Biol 2014;40:655–674.

Caussy C, Reeder SB, Sirlin CB, Loomba R. Noninvasive, quantitative assessment of liver fat by MRI-PDFF as an endpoint in NASH Trials. Hepatology 2018;68:763–772.

Cerit M, Şendur HN, Cindil E, Erbaş G, Yalçın MM, Cerit ET, Allahverdiyeva S, Oktar S, Yücel C. Quantification of liver fat content with ultrasonographic attenuation measurement function: Correlation with unenhanced multidimensional computerized tomography. Clin Imaging 2020;65:85–93.

Chanamai R, McClements DJ. Ultrasonic attenuation of edible oils. J Am Oil Chem Soc 1998;75:1447–1448.

Chen CF, Robinson DE, Wilson LS, Griffiths KA, Manoharan A, Doust BD. Clinical sound speed measurement in liver and spleen in vivo. Ultrason Imaging 1987;9:221–235.

Christensen RM. Viscoelastic properties of heterogeneous media. J Mech Phys Solids 1969;17:23–41.
D'Hondt A, Rubesova E, Xie H, Shamdasani V, Barth RA. Liver fat quantification by ultrasound in children: a prospective study. AJR Am J Roentgenol 2021;217:996–1006.
Diehl AM, Day C. Cause, pathogenesis, and treatment of nonalcoholic steatohepatitis. N Engl J Med 2017;377:2063–2072.
Dioguardi Burgio M, Imbault M, Ronot M, Faccinetto A, Van Beers BE, Rautou PE, Castera L, Gennisson JL, Tanter M, Vilgrain V. Ultrasonic adaptive sound speed estimation for the diagnosis and quantification of hepatic steatosis: a pilot study. Ultraschall Med 2019;40:722–733.
Dioguardi Burgio M, Ronot M, Reizine E, Rautou PE, Castera L, Paradis V, Garteiser P, Van Beers B, Vilgrain V. Quantification of hepatic steatosis with ultrasound: Promising role of attenuation imaging coefficient in a biopsy-proven cohort. Eur Radiol 2020;30:2293–2301.
Ferraioli G, Maiocchi L, Raciti MV, Tinelli C, De Silvestri A, Nichetti M, De Cata P, Rondanelli M, Chiovato L, Calliada F, Filice C. Detection of liver steatosis with a novel ultrasound-based technique: A pilot study using mri-derived proton density fat fraction as the gold standard. Clin Transl Gastroenterol 2019;10:e00081.
Ferraioli G, Berzigotti A, Barr RG, Choi BI, Cui XW, Dong Y, Gilja OH, Lee JY, Lee DH, Moriyasu F, Piscaglia F, Sugimoto K, Wong GL, Wong VW, Dietrich CF. Quantification of liver fat content with ultrasound: A WFUMB position paper. Ultrasound Med Biol 2021;47:2803–2820.
Fujiwara Y, Kuroda H, Abe T, Ishida K, Oguri T, Noguchi S, Sugai T, Kamiyama N, Takikawa Y. The B-mode image-guided ultrasound attenuation parameter accurately detects hepatic steatosis in chronic liver disease. Ultrasound Med Biol 2018;44:2223–2232.
Fung YC. Biomechanics: Mechanical properties of living tissues. New York: Springer-Verlag; 1981.
Ghoshal G, Lavarello RJ, Kemmerer JP, Miller RJ, Oelze ML. Ex vivo study of quantitative ultrasound parameters in fatty rabbit livers. Ultrasound Med Biol 2012;38:2238–2248.
Gu J, Liu S, Du S, Zhang Q, Xiao J, Dong Q, Xin Y. Diagnostic value of MRI-PDFF for hepatic steatosis in patients with non-alcoholic fatty liver disease: A meta-analysis. Eur Radiol 2019;29:3564–3573.
Hayashi N, Tamaki N, Senda M, Yamamoto K, Yonekura Y, Torizuka K, Ogawa T, Katakura K, Umemura C, Kodama M. A new method of measuring in vivo sound speed in the reflection mode. J Clin Ultrasound 1988;16:87–93.
Imbault M, Faccinetto A, Osmanski BF, Tissier A, Deffieux T, Gennisson JL, Vilgrain V, Tanter M. Robust sound speed estimation for ultrasound-based hepatic steatosis assessment. Phys Med Biol 2017;62:3582–3598.
Imbault M, Dioguardi Burgio M, Faccinetto A, Ronot M, Bendjador H, Deffieux T, Triquet EO, Rautou PE, Castera L, Gennisson JL, Vilgrain V, Tanter M. Ultrasonic fat fraction quantification using in vivo adaptive sound speed estimation. Phys Med Biol 2018;63 215013.
Jaeger M, Robinson E, Akarçay HG, Frenz M. Full correction for spatially distributed speed-of-sound in echo ultrasound based on measuring aberration delays via transmit beam steering. Phys Med Biol 2015;60:4497–4515.
Jayakumar S, Middleton MS, Lawitz EJ, Mantry PS, Caldwell SH, Arnold H, Mae Diehl A, Ghalib R, Elkhashab M, Abdelmalek MF, Kowdley KV, Stephen Djedjos C, Xu R, Han L, Mani Subramanian G, Myers RP, Goodman ZD, Afdhal NH, Charlton MR, Sirlin CB, Loomba R. Longitudinal correlations between MRE, MRI-PDFF, and liver histology in patients with non-alcoholic steatohepatitis: Analysis of data from a phase II trial of selonsertib. J Hepatol 2019;70:133–141.
Jeon SK, Lee JM, Joo I, Yoon JH, Lee DH, Lee JY, Han JK. Prospective evaluation of hepatic steatosis using ultrasound attenuation imaging in patients with chronic liver disease with magnetic resonance imaging proton density fat fraction as the reference standard. Ultrasound Med Biol 2019;45:1407–1416.
Jeon SK, Lee JM, Joo I. Clinical feasibility of quantitative ultrasound imaging for suspected hepatic steatosis: Intra- and inter-examiner reliability and correlation with controlled attenuation parameter. Ultrasound Med Biol 2021;47:438–445.
Koizumi Y, Hirooka M, Tamaki N, Yada N, Nakashima O, Izumi N, Kudo M, Hiasa Y. New diagnostic technique to evaluate hepatic steatosis using the attenuation coefficient on ultrasound B mode. PloS One 2019;14 e0221548.
Lin T, Ophir J, Potter G. Correlations of sound speed with tissue constituents in normal and diffuse liver disease. Ultrason Imaging 1987;9:29–40.
Napolitano D, Chou CH, McLaughlin G, Ji TL, Mo L, DeBusschere D, Steins R. Sound speed correction in ultrasound imaging. Ultrasonics 2006;44(Suppl 1):e43–e46.
Ormachea J, Parker KJ. Reverberant shear wave phase gradients for elastography. Phys Med Biol 2021;66 175001.
Parker KJ, Ormachea J. The quantification of liver fat from wave speed and attenuation. Phys Med Biol 2021;66 145011.
Parker KJ, Ormachea J, Drage MG, Kim H, Hah Z. The biomechanics of simple steatosis and steatohepatitis. Phys Med Biol 2018;63 105013.
Pirmoazen AM, Khurana A, El Kaffas A, Kamaya A. Quantitative ultrasound approaches for diagnosis and monitoring hepatic steatosis in nonalcoholic fatty liver disease. Theranostics 2020;10:4277–4289.
Robinson DE, Chen F, Wilson LS. Measurement of velocity of propagation from ultrasonic pulse-echo data. Ultrasound Med Biol 1982;8:413–420.
Shigemoto H, Sugimoto T, Hachiya H, Ebara M, Fukuda H, Kato K, Ando H. Measurement of acoustic property distributions of diseased heart and liver tissues. Japanese J Appl Phys 2001;40:3907–3911.
Stähli P, Kuriakose M, Frenz M, Jaeger M. Improved forward model for quantitative pulse-echo speed-of-sound imaging. Ultrasonics 2020;108 106168.
Stine JG, Munaganuru N, Barnard A, Wang JL, Kaulback K, Argo CK, Singh S, Fowler KJ, Sirlin CB, Loomba R. Change in MRI-PDFF and histologic response in patients with nonalcoholic steatohepatitis: A systematic review and meta-analysis. Clin Gastroenterol Hepatol 2021;19:2274–2283 e5.
Tada T, Kumada T, Toyoda H, Yasuda S, Sone Y, Hashinokuchi S, Ogawa S, Oguri T, Kamiyama N, Chuma M, Akita T, Tanaka J. Liver stiffness does not affect ultrasound-guided attenuation coefficient measurement in the evaluation of hepatic steatosis. Hepatol Res 2020;50:190–198.
Tamaki N, Koizumi Y, Hirooka M, Yada N, Takada H, Nakashima O, Kudo M, Hiasa Y, Izumi N. Novel quantitative assessment system of liver steatosis using a newly developed attenuation measurement method. Hepatol Res 2018;48:821–828.
Wang X, Alexander M, Audiere S, Baiu CX, Bamber J, Bigelow T, Carson P, Chauhan A, Chen S, Chen Y, Cloutier G, de Korte C, Engel A, Erpelding T, Esquivel-Sirvent R, Fowlkes B, Gao J, Gay J, Hah Z, Hall T, Henry JP, Lex A, Liu T, Lynch T, Mamou J, Managuli R, Mankowski-Gettle L, McAleavey S, McLauglin G, Milkowski A, Nam K, Ng G, Obuchowski N, Ormachea J, Ouhda S, Robbin M, Rogozinski B, Rubin J, Sandrin L, Sanyal AJ, Sidhu P, Thomenius K, Thornton M, Zagzebski J, Barr R, Ferraioli G, Kumar V, Ozturk A, Han A, Lavarello R, Tuthill T, Fetzer D, Stiles T, Rosado-Mendez I, Wang M, Samir A, Rosenzweig S, Pierce T. Speed of sound measurement to quantify hepatic steatosis: An AIUM/QIBA perspective. Presented at the 45th Annual International Symposium on Ultrasonic Imaging and Tissue Characterization, QIBA Session 2, Virtual Meeting. .
Yoo J, Lee JM, Joo I, Lee DH, Yoon JH, Kang HJ, Ahn SJ. Reproducibility of ultrasound attenuation imaging for the noninvasive evaluation of hepatic steatosis. Ultrasonography 2020;39:121–129.
Zhang M, Castaneda B, Wu Z, Nigwekar P, Joseph JV, Rubens DJ, Parker KJ. Congruence of imaging estimators and mechanical measurements of viscoelastic properties of soft tissues. Ultrasound Med Biol 2007;33:1617–1631.